PHYSICAL REVIEW B **84**, 121308(R) (2011)

# Accurate electronic properties for (Hg,Cd)Te systems using hybrid density functional theory

Jeremy W. Nicklas* and John W. Wilkins
*Department of Physics, The Ohio State University, Columbus, Ohio 43210, USA*
(Received 15 August 2011; published 27 September 2011)

Hybrid screened density functional theory better describes the electronic structure of HgTe, CdTe, and HgCdTe systems in comparison with standard density functional theory. The unique hybrid functional reproduces the band inversion in the popular HgCdTe alloy, justifying it as a better method than standard density functional theory in the search for different topological insulators. In addition, the 0.53-eV valence-band offset obtained using the hybrid functional supports the recently observed higher band offset in the HgTe/CdTe heterostructure.

DOI: 10.1103/PhysRevB.84.121308 PACS number(s): 71.20.Nr, 71.23.−k, 71.55.Gs, 71.70.Ej

*Introduction*. The $Hg_{1-x}Cd_xTe$ alloy has a narrow gap range extending up to nearly the entire infrared spectrum. It is the material of choice for many high-performance infrared detection applications. Recently it has come back under the spotlight for HgTe's topological insulating behavior. A topological insulator has an insulating energy gap in the bulk states but conducting metallic states on the edges or surface. The two-dimensional (2D) topological insulator exhibits a quantum spin Hall effect which was recently observed experimentally in HgTe/(Hg,Cd)Te quantum wells.[1,2] This has sparked an interest in finding unique topological insulators by computing and finding band inversions in the band structure using standard density functional theory (DFT).[3,4] A more accurate treatment of the band structure can be achieved using a different hybrid functional, possibly improving upon the search for such materials, as shown for multinary chalcogenides.[5]

The Heyd-Scuseria-Ernzerhof (HSE) hybrid functional,[6,7] which combines the screened exchange with the Perdew-Burke-Ernzerhof (PBE) generalized gradient approximation (GGA) functional,[8] has been seen to reproduce experimental electronic properties as well as band offsets for a range of III-V alloys.[9,10] This Rapid Communication extends upon those by reporting that HSE outperforms standard DFT on the electronic structure of the II-VI alloy $Hg_{1-x}Cd_xTe$ by reproducing the experimental crossover at $x = 0.17$ (Ref. 11) and transitioning from a semimetallic alloy with band inversion to a gapped semiconducting alloy. HSE also achieves a valence-band offset (VBO) of 0.53 eV for HgTe/CdTe(001), agreeing with the more recent experimental data and settling a controversy on the VBO.[12,13]

Figure 1(a) describes a typical cubic trivial band-gap insulator (e.g., CdTe) with spin-orbit splitting. The conduction states exhibit *s*-like orbital symmetry and the Γ point possesses $\Gamma_6$ (twofold-degenerate) symmetry. The top of the valence band exhibits *p*-like orbital symmetry with a total angular momentum of $J = 3/2$ and a Γ point with $\Gamma_8$ (fourfold-degenerate) symmetry. The split-off band below that has a total angular momentum of $J = 1/2$ with a Γ point possessing $\Gamma_7$ (twofold-degenerate) symmetry. Figure 1(b) describes a semimetal (e.g., HgTe) where now the $\Gamma_6$ bands lie below the $\Gamma_8$ bands and are fully occupied—this is referred to as band inversion. By applying a lattice distortion to the semimetal the degeneracy in the $\Gamma_8$ states is lifted, leading to a nontrivial band gap, and hence a topological insulator.

*Method*. The calculations are performed using the projector augmented-wave (PAW) method.[14] The functionals included are the PBE[8] and the HSE06[7] hybrid functional in the VASP code.[15,16] The wave functions are expanded in plane waves up to an energy cutoff of 350 eV. The Brillouin-zone integration is carried out on an $8 \times 8 \times 8$ Γ-centered $k$ mesh over the full Brillouin zone for the face-centered cubic primitive cell. Integrations over $4 \times 3 \times 3$, $3 \times 3 \times 3$, and $8 \times 8 \times 1$ Γ-centered $k$ meshes are used for the $x = 0.25$ and $x = 0.50$ special quasirandom structure (SQS) supercells and the $4 + 4$ layer (001) heterostructure supercell, respectively.

The alloys are modeled by SQSs,[17] ordered structures designed to reproduce the most important pair-correlation functions of a random alloy. We use our previously published 32-atom SQSs with Cd concentrations of 25%, 50%, and 75% for this alloy calculation.[9] The 25% and 75% SQSs, differing only by swapping Hg atoms with Cd atoms, match the pair-correlation functions of a random alloy up to third nearest neighbor and the 50% SQS matches up to seventh nearest neighbor. The lattice constants for the $Hg_{1-x}Cd_xTe$ alloy are linearly interpolated between the experimental parent compound lattice constants of HgTe ($a = 6.46$ Å) and CdTe ($a = 6.48$ Å).[18] Relaxation is not taken into account due to the small lattice mismatch.

The heterostructure is described by a $4 + 4$ layer thick supercell of 16 atoms with a (001) interface. An average of the experimental lattice constants of HgTe and CdTe is chosen as the lattice constant of the heterostructure. We employ the average electrostatic potential technique[19] to compute the VBO of the heterostructure as

$$\mathrm{VBO} = \Delta E_{\mathrm{VBM}}^{(\mathrm{HgTe-CdTe})} - \Delta V_{\mathrm{step}}^{(\mathrm{HgTe-CdTe})}, \qquad (1)$$

where $\Delta E_{\mathrm{VBM}}$ is the difference in the valence-band maxima of the bulk HgTe and bulk CdTe and $\Delta V_{\mathrm{step}}$ is the discontinuity in the reference potential across the heterostructure interface.

*Results*. Figure 2 shows the projected band structure for both CdTe and HgTe obtained using the PBE and HSE functional with the top of the valence band set at 0 eV. The *s*-like projections are denoted by red circles with the weight of the projection being symbolized by the size of the circle. The $\Gamma_6$ projection is given by the solid red circle. Going from PBE to HSE the $\Gamma_6$ band is pushed upward in both materials to at or near the correct experimental values. In the case of HgTe it

 

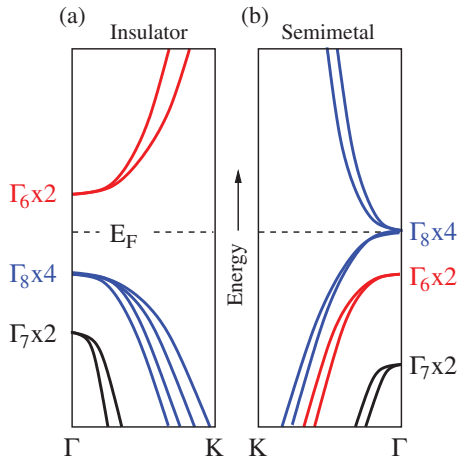


FIG. 1. (Color online) Schematic diagram of the band structure near the Γ point for (a) a cubic trivial band-gap insulator and (b) a semimetal. The bands below the Fermi level (dashed line) are filled and the ones above are empty. For a semimetal the *s*-like $\Gamma_6$ states lie below the Fermi level and are filled, whereas the *p*-like $\Gamma_8$ bands now form the top of the valence and bottom of the conduction band.

reproduces the correct ordering of the $\Gamma_8$, $\Gamma_6$, and $\Gamma_7$ bands, respectively, whereas PBE reverses the ordering of the $\Gamma_6$ and $\Gamma_7$.

Table I compares the calculated band gaps and spin-orbit splittings for both CdTe and HgTe against experiment. For discussion, the band gap is taken as the energy difference between $\Gamma_6$ and $\Gamma_8$. For the case of a semimetal the band gap will be "negative." The HSE functional yields band gaps and splitting energies closer in magnitude to experiment than PBE for both materials. Even though HSE was initially developed to compute accurate band gaps for semiconductors in mind, it still manages to reproduce the negative band-gap value for HgTe.

The band gap ($\Gamma_6 - \Gamma_8$ energy difference) versus Cd concentration for the $Hg_{1-x}Cd_xTe$ alloy is plotted in Fig. 3. A cubic fit is used for the five data points taken at the end

TABLE I. The band-gap energy ($E_g = E_{\Gamma_6} - E_{\Gamma_8}$) and spin-orbit splitting energy ($\Delta_0 = E_{\Gamma_8} - E_{\Gamma_7}$) in units of eV for both CdTe and HgTe computed using both HSE and PBE, compared with experiment. Note that although HSE tends to underestimate the CdTe band gap by 16%, in stark contrast, PBE underestimates it by 68%.

| | HSE | PBE | Expt. |
|---|---|---|---|
| CdTe | | | |
| $E_g$ | 1.34 | 0.52 | 1.6[a] |
| $\Delta_0$ | 0.92 | 0.84 | 0.95[b] |
| HgTe | | | |
| $E_g$ | −0.27 | −0.93 | −0.29[c] |
| $\Delta_0$ | 0.89 | 0.76 | 0.91[c] |

[a]From Ref. 20.
[b]From Ref. 21.
[c]From Ref. 22.

points and Cd concentrations of 25%, 50%, and 75% for the calculated values. The HSE fit lies nearly on top of the experimental fit[11] for smaller concentrations of Cd while slightly underestimating the magnitude at higher concentrations. PBE grossly underestimates this band gap while failing to predict it as a semiconducting alloy throughout much of the alloy range.

Table II lists the computed Cd compositions at which the $Hg_{1-x}Cd_xTe$ alloy goes from semimetallic to a trivial band-gap semiconductor. HSE reproduces the experimental crossover to two significant figures. The ability to predict band inversion across an entire alloy has major implications in the search for unique topological insulators. Standard density functional theory such as PBE tends to underestimate the band gap as seen here, and this can lead to the prediction of false positives when looking for topological insulators.

The VBO is calculated for the HgTe/CdTe(001) interface using HSE. The HSE functional yields a VBO of 0.53 eV in contrast to previous self-consistent calculations of 0.27 eV,[24] 0.22 eV,[25] and 0.37 eV.[26] HSE is in excellent agreement with the more recent experimental values of $0.53 \pm 0.06$ eV (Ref. 12) and $0.55 \pm 0.05$ eV,[13] in contradiction with earlier

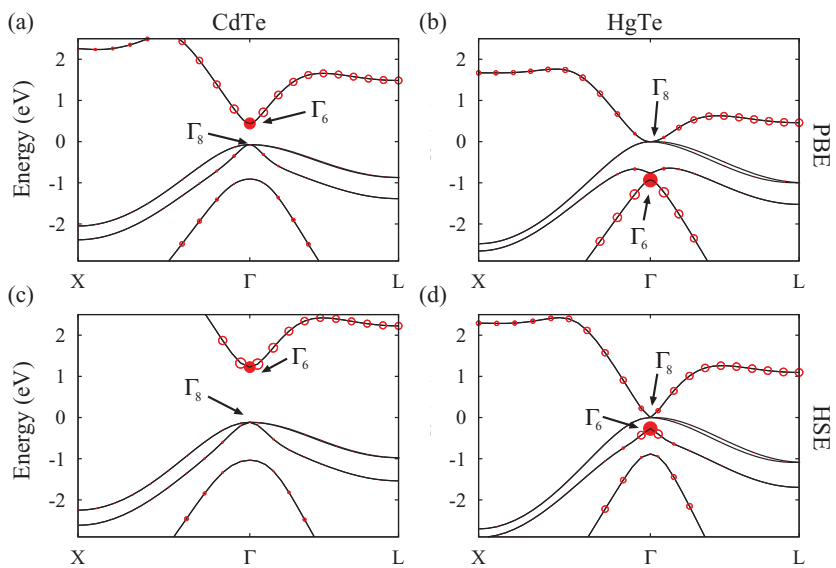


FIG. 2. (Color online) Projected band-structure plots of the *s*-like state for (a) CdTe and (b)HgTe using PBE, as well as (c) CdTe and (d) HgTe using HSE. The sizes of the circles correspond to the weight of the *s*-like projection. The filled circle corresponds to the *s*-like projection at the Γ point, $\Gamma_6$. Arrows and proper labels point to the $\Gamma_6$ and $\Gamma_8$ locations in the band structures. HSE accurately reproduces the band-gap energy ($E_g = E_{\Gamma_6} - E_{\Gamma_8}$) for both CdTe and HgTe.

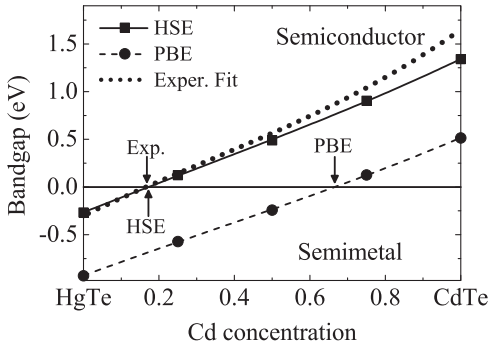


FIG. 3. Band gap (defined as $E_{\Gamma_6} - E_{\Gamma_8}$) vs alloy concentration of $Hg_{1-x}Cd_xTe$ computed using HSE (solid line) and PBE (dashed line) compared to experiment (dotted line) (Ref. 11). A positive band gap corresponds to a trivial gap semiconductor and a negative band gap corresponds to a semimetal. The data points used for the fits are shown as squares and circles for HSE and PBE, respectively. The crossovers from semimetal to semiconductor for each functional and experiment are labeled by arrows. HSE agrees with experiment for not only the band-gap magnitude but also the alloy's transition from a semimetal to a normal gap semiconductor.

x-ray and ultraviolet photoelectron spectroscopy which provide a VBO of ∼0.35 eV.[27–29] Eich *et al.*[12] demonstrate that an accurate treatment of the band dispersion in HgTe at the valence-band edge is necessary for a correct measurement of the VBO leading to the higher observed VBO. HSE in this case lends strong support for this higher band offset.

TABLE II. The Cd concentration in $Hg_{1-x}Cd_xTe$ at which the alloy goes from being semimetallic to a trivial band-gap semiconductor, labeled by $x_{\text{crossover}}$. HSE yields a crossover composition in very good agreement with experiment. PBE predicts the alloy to be semimetallic throughout most of the composition.

| | HSE | PBE | Expt. |
|---|---|---|---|
| $x_{\text{crossover}}$ | 0.17 | 0.67 | 0.17[a], 0.16[b] |

[a]Using the fit from Ref. 11.
[b]Using the fit from Ref. 23.

*Conclusions*. We present a hybrid functional study of the electronic properties of HgTe and CdTe. The calculated band structures using HSE show better band gaps and band ordering compared with experiment than standard DFT for bulk HgTe and CdTe. Our results confirm that (a) HSE is superior in reproducing the semimetal-to-semiconductor transition in the $Hg_{1-x}Cd_xTe$ alloy, providing a solid basis for future work in topological insulator studies, and (b) HSE strengthens the argument for a higher VBO of 0.53 eV in the HgTe/CdTe interface.

This work was supported by DOE-Basic Energy Sciences, Division of Materials Sciences (Grant No. DE-FG02-99ER45795). Computational resources were provided in part by an allocation of computing time from the Ohio Supercomputer Center and the National Energy Research Science Computing Center. The latter is supported by the Office of Science of the U.S. Department of Energy under Contract No. DE-AC02-05CH11231. We are also grateful to Amita Wadehra for her useful comments.

*nicklas.2@buckeyemail.osu.edu

[1]M. König, S. Wiedmann, C. Brüne, A. Roth, H. Buhmann, L. W. Molenkamp, X.-L. Qi, and S.-C. Zhang, Science **318**, 766 (2007).
[2]A. Roth, C. Brüne, H. Buhmann, L. W. Molenkamp, J. Maciejko, X.-L. Qi, and S.-C. Zhang, Science **325**, 294 (2009).
[3]S. Chadov, X. Qi, J. Kübler, G. H. Fecher, C. Felser, and S. C. Zhang, Nat. Mater. **9**, 541 (2010).
[4]H. Lin, L. A. Wray, Y. Xia, S. Xu, S. Jia, R. J. Cava, A. Bansil, and M. Z. Hasan, Nat. Mater. **9**, 546 (2010).
[5]S. Chen, X. G. Gong, C.-G. Duan, Z.-Q. Zhu, J.-H. Chu, A. Walsh, Y.-G. Yao, J. Ma, and S.-H. Wei, Phys. Rev. B **83**, 245202 (2011).
[6]J. Heyd, G. E. Scuseria, and M. Ernzerhof, J. Chem. Phys. **118**, 8207 (2003).
[7]J. Heyd, G. E. Scuseria, and M. Ernzerhof, J. Chem. Phys. **124**, 219906 (2006).
[8]J. P. Perdew, K. Burke, and M. Ernzerhof, Phys. Rev. Lett. **77**, 3865 (1996).
[9]J. W. Nicklas and J. W. Wilkins, Appl. Phys. Lett. **97**, 091902 (2010).
[10]A. Wadehra, J. W. Nicklas, and J. W. Wilkins, Appl. Phys. Lett. **97**, 092119 (2010).
[11]G. L. Hansen, J. L. Schmit, and T. N. Casselman, J. Appl. Phys. **53**, 7099 (1982).
[12]D. Eich, K. Ortner, U. Groh, Z. H. Chen, C. R. Becker, G. Landwehr, R. Fink, and E. Umbach, Phys. Status Solidi A **173**, 261 (1999).
[13]Z. Yang, Z. Yu, Y. Lansari, S. Hwang, J. W. Cook, and J. F. Schetzina, Phys. Rev. B **49**, 8096 (1994).
[14]P. E. Blöchl, Phys. Rev. B **50**, 17953 (1994).
[15]G. Kresse and J. Furthmuller, Phys. Rev. B **54**, 11169 (1996).
[16]G. Kresse and D. Joubert, Phys. Rev. B **59**, 1758 (1999).
[17]S.-H. Wei, L. G. Ferreira, J. E. Bernard, and A. Zunger, Phys. Rev. B **42**, 9622 (1990).
[18]T. Skauli and T. Colin, J. Cryst. Growth **222**, 719 (2000).
[19]A. Baldereschi, S. Baroni, and R. Resta, Phys. Rev. Lett. **61**, 734 (1988).
[20]*Semiconductors: Intrinsic Properties of Group IV Elements and III-V, II-VI and I-VII Compounds*, edited by O. Madelung, W. Van der Osten, and U. Rössler, Landolt-Börnstein, New Series, Group III, Vol. 22 (Springer, Berlin, 1987), p. 210.
[21]A. Twarkdowski, E. Rokita, and J. A. Gaj, Solid State Commun. **36**, 927 (1980).
[22]N. E. Orlowski, J. Augustin, Z. Golacki, C. Janowitz, and R. Manzke, Phys. Rev. B **61**, R5058 (2000).
[23]J. Chu, S. Xu, and D. Tang, Appl. Phys. Lett. **43**, 1064 (1983).
[24]N. E. Christensen, Phys. Rev. B **38**, 12687 (1988).
[25]A. Qteish and R. J. Needs, Phys. Rev. B **47**, 3714 (1993).
[26]S.-H. Wei and A. Zunger, Phys. Rev. Lett. **59**, 144 (1987).
[27]S. P. Kowalczyk, J. T. Cheung, E. A. Kraut, and R. W. Grant, Phys. Rev. Lett. **56**, 1605 (1986).
[28]R. S. Sporken, S. Sivananthan, J. P. Faurie, D. H. Ehlers, J. Fraxedos, L. Ley, J. J. Pireaux, and R. Caudano, J. Vac. Sci. Technol. A **7**, 427 (1989).
[29]C. K. Shih and W. E. Spicer, Phys. Rev. Lett. **58**, 2594 (1987).